energies

MDPI

Article

A Double-Bed Adsorptive Heat Transformer for Upgrading Ambient Heat: Design and First Tests

Mikhail Tokarev

Boreskov Institute of Catalysis, Ac. Lavrentiev av. 5, 630090 Novosibirsk, Russia; tokarev@catalysis.ru

Received: 28 September 2019; Accepted: 22 October 2019; Published: 23 October 2019

Abstract: A full scale lab prototype of an adsorptive heat transformer (AHT), consisting of two adsorbers, an evaporator, and a condenser, was designed and tested in subsequent cycles of heat upgrading. The composite $LiCl/SiO_2$ was used as an adsorbent with methanol as an adsorbtive substance under boundary temperatures of $T_L/T_M/T_H$ = −30/20/30 °C. Preliminary experiments demonstrated the feasibility of the tested AHT in continuous heat generation, with specific power output of 520 W/kg over 1–1.5 h steady-state cycling. The formal and experimental thermal efficiency of the tested rig were found to be 0.5 and 0.44, respectively. Although the low potential heat to be upgraded was available for free from a natural source, the electric efficiency of the prototype was found to be as high as 4.4, which demonstrates the promising potential of the "heat from cold" concept. Recommendations for further improvements are also outlined and discussed in this paper.

Keywords: adsorptive heat transformation; heat upgrading; composite adsorbent; methanol; useful heat; specific power

1. Introduction

Adsorptive heat transformation (AHT) is an energy-saving and environmentally friendly technology that is attracting increasing attention due to its ability to effectively convert and store waste or renewable heat [1–3]. The adsorption cooling [4], deep freezing [5], ice production [6], air conditioning [7], heat pumping and storage [8] have attracted a lot of research in recent decades. Nowadays, several adsorptive chillers and heat pumps are available on the market [2,9]. However, the adsorptive technologies for temperature level upgrading and heat amplification are not well-developed.

Recently, a novel adsorption cycle called "heat from cold" (HeCol) was suggested for upgrading ambient heat [10]. The HeCol cycle consists of two isosteres (1-2, 3-4) and two isotherms (2-3, 4-1), and operates between three thermostats at low (T_L), middle (T_M), and high (T_H) temperatures (Figure 1). The lowest temperature is that of the surrounding atmosphere, which in winter can be as low as −10 to −60 °C, especially in the northern regions. The thermostat at middle temperature represents a natural source of low-potential heat, and commonly T_M ranges between 0 and 20 °C. The soil, underground water, or other natural reservoirs of nonfreezing water can be used as the middle temperature thermostat. The thermostat at T_H serves as a heat consumer. The novelty of the HeCol cycle is that the adsorbent regeneration is initiated by the drop in vapor pressure over the adsorbent down to P_L (4 → 1), whereas in the common AHT desorption is driven by the adsorbent heating. For this purpose, the condenser is maintained at low temperature (T_L), while the adsorbent is maintained at middle temperature T_M and the heat for desorption is used for free from the natural heat source.

The useful heat generation proceeds isothermally at high cycle temperature T_H (2 → 3) and is initiated by vapor pressure increase to P_M. At this stage, the evaporator is kept at middle temperature; thus, heat for evaporation comes from the natural heat source. The nonisothermal version of the HeCol cycle can be realized also (2 → 3* → 3), as is shown in Figure 1. In this case, less heat is supplied to the consumer, however, at a higher temperature. After the adsorption and regeneration stages are

complete, the adsorptive that is collected in the condenser should be pumped back into the evaporator. The estimations presented in [11,12] demonstrate that the mechanical work needed for pumping is negligible. A detailed description and analysis of the HeCol cycle can be found elsewhere [11].

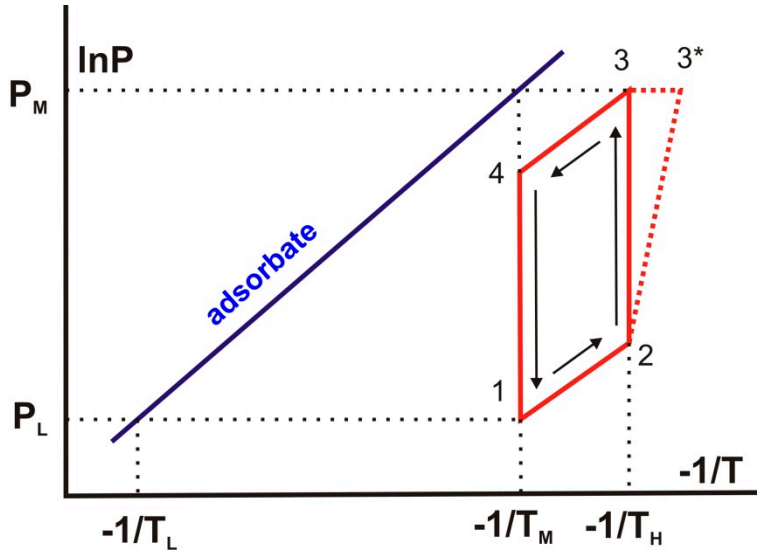

Figure 1. P-T diagram of the "heat from cold" (HeCol) cycle.

The first lab-scale HeCol prototype was built and tested with three methanol sorbents, namely the carbon ACM-35.4 [12] and composites $CaClBr/SiO_2$ [13] and $LiCl/SiO_2$ [14], to evaluate the cycle performance and output characteristics. Thus, the possibility of practical realization of the HeCol cycle was approved experimentally. It was shown that desorption and adsorption are driven by pressure drop and jump, respectively, which take place at a rate sufficient to reach the maximal specific adsorption power. This can be as high as SP_{ads} = 6–8 kW/kg, with a maximal temperature of T_{max} = 53 °C. Although the first prototype demonstrated a high formal efficiency of about 0.5, it operated in intermittent mode and consisted of only a single adsorber, with a single chamber serving as the condenser and evaporator. Achieving further progress with the HeCol concept, evidently, calls for realization of continuous heat generation under repeatable and steady-state cycling.

In this paper, the author presents a full-scale HeCol prototype capable of continuous operation. The design of the test rig is described in detail. Then, the experimental procedures are listed and the first experimental results are presented, demonstrating the performance and output characteristics of the tested prototype. Finally, the effect of the cycle duration is studied and the suggestions for further improvements are outlined.

2. Materials and Methods

2.1. The Test Rig

The experimental rig is presented in Figure 2. The main parts of the prototype are the two adsorbers, the evaporator, and the condenser (Figure 2a,b). Each adsorber contains 2 aluminum-fined, flat-tube heat exchangers (HExes) from Yamaha Aerox (Yamaha Corporation, Shizuoka, Japan), filled with loose grains (0.2–0.5 mm) of $LiCl/SiO_2$ composite adsorbent (Figure 2c) [15]. The adsorbent loading of each adsorber equals 500 ± 0.2 g. The adsorbent is placed in a free space between primary and secondary heat exchange elements and fixed with a stainless steel net, as demonstrated in Figure 2c. The total mass of the adsorbent loaded in the experimental rig is m = 1.0 ± 0.0004 kg.

The evaporator and condenser are flat rectangle chambers with dimensions of 50 cm × 25 cm × 10 cm. Inside each chamber, a couple of fined, flat-tube HExes are installed in order to maintain fixed methanol temperature and pressure (Figure 2d).

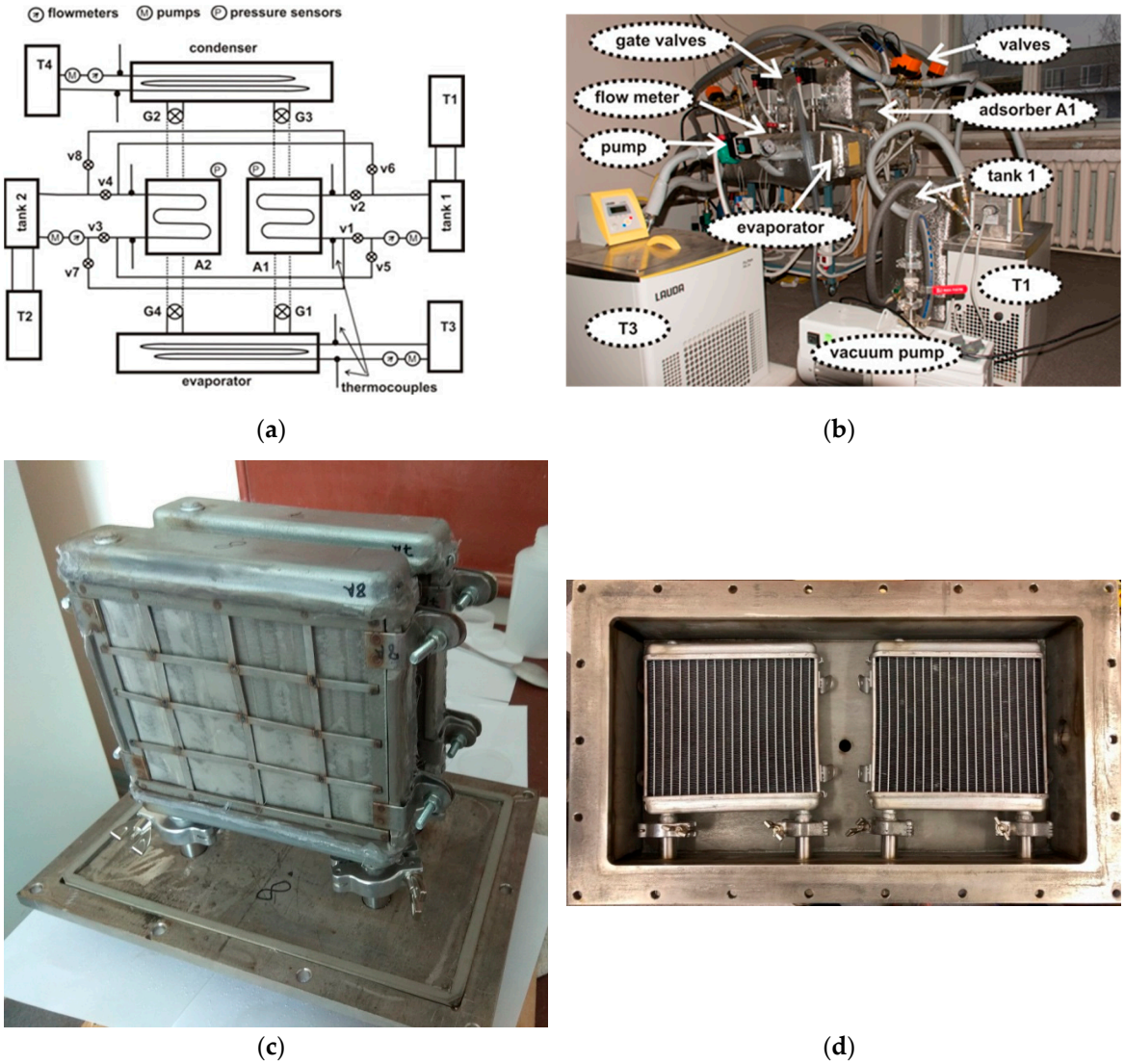

Figure 2. (**a**,**b**) The experimental rig. Note: T1–T4: thermocryostats; A1, A2: adsorbers; v1–v8: valves; G1–G4: gate valves. Adsorber (**c**) and evaporator (**d**) with installed heat exchangers.

The adsorbers, evaporator, and condenser are connected by 4 electromechanical VAT-264 (VAT Group AG, Sennwald, Switzerland) vacuum gate valves (Figure 2a,b), in a way that each adsorber is coupled with both the evaporator and condenser. The vacuum pump (Figure 2b) serves to evacuate the chambers before the tests.

To maintain the boundary cycle temperatures T_L, T_M, and T_H, the four thermocryostats T1, T2, T3, and T4 (Figure 2a,b) are used. For this purpose, the evaporator is connected to thermocryostat T3 and is kept at the middle cycle temperature T_M, while cryostat T4 cools the condenser down to the lowest cycle temperature T_L, as is shown in Figure 2a. Thermostats T1 and T2 are equipped with 30 dm^3 buffer tanks (Figure 2b) and imitate the heat consumer (at T_H) and the source of low potential heat (at T_M), correspondingly.

The evaporator, condenser, and adsorbers are connected to the thermocryostats and tanks by the circuits, which consist of the pipelines, pumps, and electromechanical valves (Figure 2a,b). The impeller-type rotameters serve to control the flow rate f of thermal liquid inside the circuits.

The condenser circuit is filled with 40% ethylene glycol/water mixture, while distilled water is used in the circuits for the evaporator and adsorbers. The flow rate of the thermal liquid for the adsorbers' circuit is f = 400 L/h, for the evaporator is f = 535 L/h, and for the condenser is f = 400 L/h.

The vapor pressure P inside the adsorbers is controlled by Brooks CMC gauges (Brooks Instrument, Hatfield, PA, USA). The temperature of the thermal liquid at the inlet T_{in} and outlet T_{out} of the condenser, evaporator, and the adsorbers is measured by K-type thermocouples. All the sensors are connected to the computer-controlled analog-to-digital converter (ADC), which allows data collection every 1 ± 0.005 s. After connecting the thermocouples to the individual ADC ports, they are calibrated with the use of a specialized thermal bath that ensures the accuracy of T readings to ± 0.1 K. The electromechanical vacuum gates, valves, and pumps are connected to the computer-controlled digital-to-analog converters (power relays) and are switched on or off according to the working diagram presented in Table 1. Thermal insulation on the test rig (Figure 2b) serves to prevent heat loss.

Table 1. Working diagram of the test rig.

N	Operating Mode	Duration [1], s	Position				
			Gates G1, G2	Gates G3, G4	Valves v1–v4	Valves v5–v8	Pumps M1, M2
0	All closed	-	closed	closed	closed	closed	off
I	Half-cycle 1 Isosteric heating–cooling	100	closed	closed	opened	closed	on
II	Half-cycle 1 Adsorption/desorption	100–400	opened	closed	opened	closed	on
III	Half-cycle 1 equilibration	100	closed	closed	opened	closed	on
IV	Half-cycle 2 Isosteric heating–cooling	100	closed	closed	closed	opened	on
V	Half-cycle 2 Adsorption/desorption	100–400	closed	opened	closed	opened	on
VI	Half-cycle 2 equilibration	100	closed	closed	closed	opened	on

[1] The whole cycle duration is 600–1200 s.

2.2. Experimental Procedure

Before tests, the adsorbers are heated up to 90 °C and pumped at P < 0.1 mbar over 2 h, in order to regenerate the adsorbent and to remove the residual air from the chambers. Then, the adsorbers are cooled down to room temperature. The evaporator and condenser are evacuated as well, and then the evaporator is filled with 5 kg of pure and degassed methanol. Then, the boundary cycle temperatures are set as follows: $T_{cond} = T_L = -30$ °C, $T_{ev} = T_M = 20$ °C, $T_{ads} = T_H = 30$ °C, $T_{des} = T_M = 20$ °C. After reaching the boundary temperatures, the test rig is ready for continuous cycling.

A single complete cycle consists of two half-cycles. During the first half-cycle, adsorber A1 is maintained at $T = T_H$ and is in contact with the evaporator, while adsorber A2 is connected to the condenser at temperature $T = T_M$. During the second half-cycle, the adsorbers operate in opposite mode. Each individual half-cycle consists of 3 steps: isosteric heating–cooling, adsorption–desorption, and thermal equilibration (Table 1).

In the first step, valves v1–v4 are opened and pumps M1 and M2 are turned on. The flow of heat transfer fluid (HTF) at temperature T_H passes though adsorber A1, while adsorber A2 is kept at T_M, as schematically shown in Figure 3a. After adsorbers A1 and A2 reach T_H and T_M, respectively, gates G1 and G2 are opened. Thus, adsorber A1 is connected to the evaporator and adsorber A2 is in contact with the condenser, and the adsorption–regeneration step is started. Then, the gates are closed, while the HTF continues to pass through the adsorbers. At this stage, adsorbers A1 and A2 are not in contact with adsorptive and return to thermal equilibrium at T_H and T_M, respectively. After finishing the third step, the first half-cycle is completed. The second half-cycle is organized in the same

sequence; however, valves v1–v4 are closed and valves v5–v8 are activated to arrange the HTF flow in a way that adsorber A1 is kept at T = T_M and adsorber A2 is connected to the consumer circuit at T = T_H (Figure 3b). Opening gates G3 and G4 leads to the beginning of the adsorption–regeneration step, whereas closing the vacuum gates is followed by thermal equilibration of the adsorbers. Hence, step-by-step activation of the operating modes from steps I–VI leads to a complete HeCol cycle being performed, as outlined in Table 1.

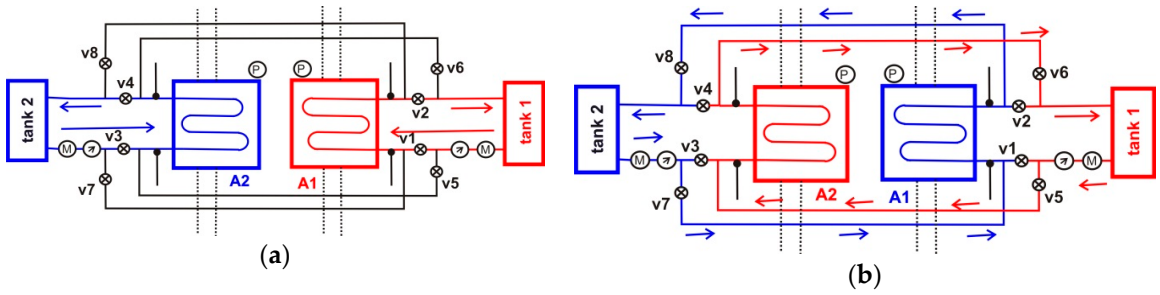

Figure 3. Scheme of thermal liquid flow during the first (**a**) and second (**b**) half-cycles, according to the working diagram (Table 1). Tank 1 is maintained at T = T_H and tank 2 at T = T_M.

The duration of both the isosteric and equilibration steps is 100 s, in order to ensure the accurate separation of thermal effects caused by adsorption–desorption with those resulting from switching the direction of the HTF flow inside the HExes. The duration $t_{ads/des}$ of the adsorption–desorption step varies from 100 to 400 s. Thus, the total duration of the cycle varies from 600 to 1200 s, as is indicated in Table 1. The complete cycle is repeated continuously 8–12 times over the course of the experiments.

2.3. Data Evaluation

Heat flow W in the adsorbers, evaporator, and condenser is evaluated as follows:

$$W = (T_{out} - T_{in}) \times f \times \rho \times Cp/3.6, \quad (1)$$

where ρ and Cp are the density and specific heat of HTF, and T_{in} and T_{out} are the temperatures at the inlet and outlet, respectively.

Integration of W gives the thermal effect Q:

$$Q = \int W dt, \quad (2)$$

The density of the HTF was measured at a constant temperature of 25 °C, using a standard lab densimeter with ±0.01 g/cm^3 accuracy. The heat capacity of the thermal liquid at appropriate temperatures T_L, T_M, and T_H was evaluated by means of SecCool Properties software [16], within ± 2% uncertainty.

2.4. Error Analysis

The determination of heat fluxes is based on the simultaneous measurements of the temperature difference and flow rate of the HTF. Thus, the instrumental uncertainties in T_{in}, T_{out}, and f contribute to the cumulative error, as well as the errors of density and heat capacity of HTF. The resulting relative error of power W and heat Q was estimated as δ(W) = δ(Q) = ± 9%, as is listed in Table 2.

Table 2. The measurement uncertainties and error analysis.

N	Source Of Uncertainty And Instrumental Error	Relative δ [%] and Absolute ε [K], [g/cm^3] Errors	Relative Error δ [%] of W and Q
1	Thermocouple and analog-to-digital converter (ADC) ± 0.1 K	$\Delta T = T_{out} - T_{in}$ $\varepsilon(\Delta T) = 2 \times \varepsilon(T) = 0.2$ K $\Delta T = 5$ K $\delta(\Delta T) = 0.2 / 5 \times 100\% = 4$ %	$W \sim (\Delta T) \times f \times \rho \times Cp$ $Q \sim W$ $\delta(W) = \delta(Q) = \delta(\Delta T) + \delta(f) + \delta(\rho) + \delta(C_p) =$ **9%**
2	Flow meter ± 2 %	$\delta(f) = 2\%$	
3	Densimeter ± 0.01 g/cm^3	$\varepsilon(\rho) = 0.01$ g/cm^3 $\rho \approx 1$ g/cm^3 $\delta(\rho) = 0.01/1 \times 100\% = 1\%$	
4	Heat capacity ± 2 %	$\delta(C_p) = 2\%$	

3. Results and Discussion

3.1. Case Study

The adsorption and regeneration processes in the HeCol cycle are driven by pressure jump or drop, respectively. Figure 4a shows that the temporal pressure evolution in the adsorbers after just two complete cycles reaches a steady state. Then, after 1–1.5 h of cycling, the amplitude of pressure jumps or drops reduces visibly, which is caused by the fact that the level of methanol in the evaporator becomes too low and the evaporation pressure gradually decreases. For the cycles with a longer adsorption–desorption step, the steady-state regime is achieved just after the first complete cycle (Figure 4b).

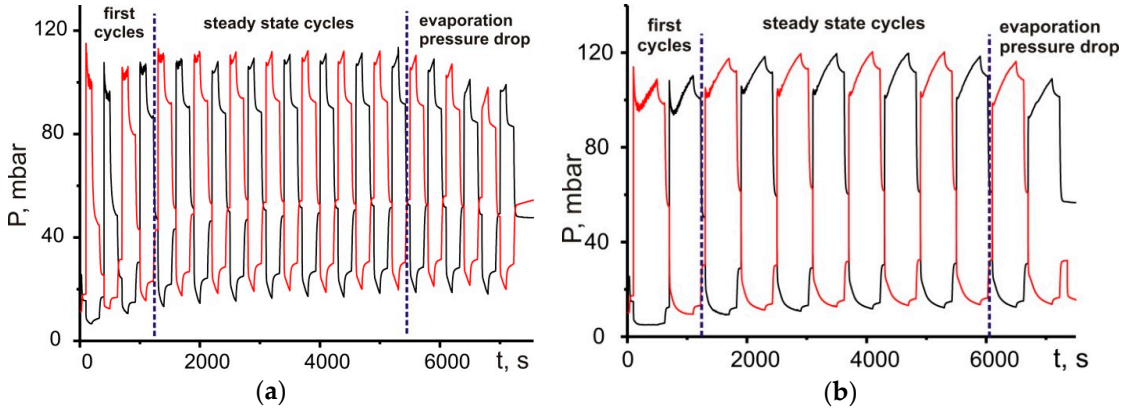

Figure 4. Temporal evolution of methanol pressure in adsorbers A1 (red) and A2 (black). The durations of the adsorption–desorption stages are 100 s (**a**) and 400 s (**b**).

The dependence of thermal power consumed in evaporator W_{ev} or released in condenser W_{con} (Figure 5) follows the same tendency and reaches a steady-state regime after performing the first 1–2 complete cycles. Maximal thermal power for both evaporation and condensation reaches W_{max} ~ 1.5 kW. The total heat consumed in the evaporator over the course of 4 consecutive steady-state cycles (t = 1400–6000 s, Figure 5a) is Q_{ev} = 2170 kJ. The total heat released in the condenser (Figure 5b) of Q_{con} = 2150 kJ is close to evaporation heat Q_{ev}; consequently, in a steady-state regime, both the evaporator and condenser demonstrate repeatable operation. Taking into account the latent enthalpy of methanol evaporation $\Delta H_{ev} = 1.1 \times 10^6$ J/kg [17], it is easy to calculate the amount of methanol exchanged in a single complete cycle:

$$\Delta w = Q_{ev}/(\Delta H_{ev} \times m \times 4) = 0.49 \text{ kg/kg}. \quad (3)$$

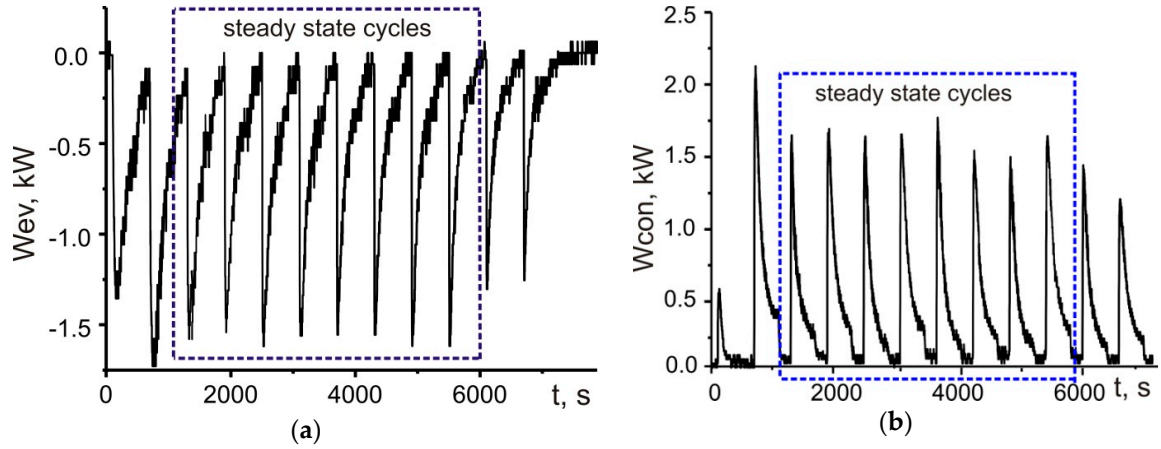

Figure 5. Thermal power consumed in the evaporator (**a**) and released in the condenser (**b**). The duration of the adsorption–desorption stage is 400 s.

The evolution of the inlet and outlet temperatures for adsorbers is presented in Figure 6. This confirms that when operating in an opposite mode, both adsorbers A1 and A2 demonstrate identical behavior over the steady-state period. The experimental cycles presented in the P-T diagram (Figure 7) for adsorbers A1 (red line) and A2 (black line) coincide as well.

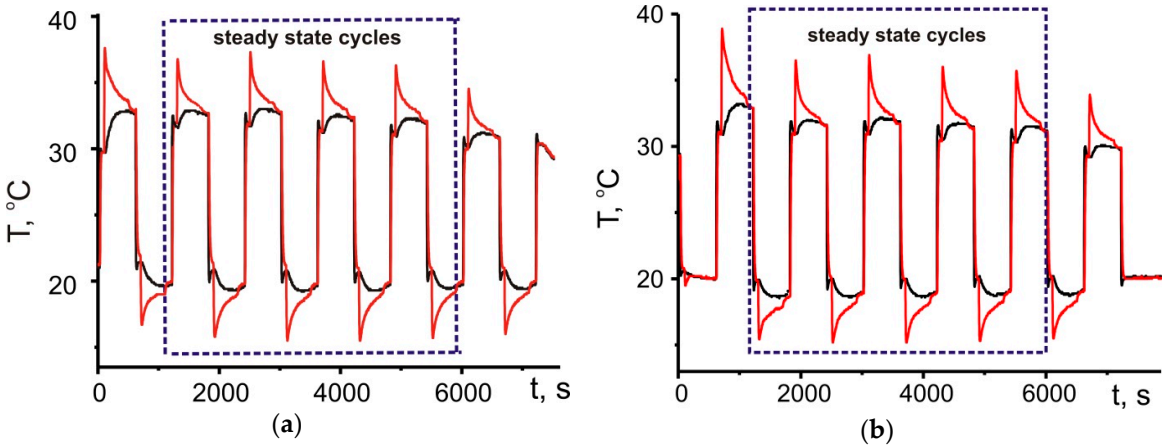

Figure 6. Temperature at the inlet (black) and outlet (red) of adsorbers A1 (**a**) and A2 (**b**). The duration of the adsorption–desorption stage is 400 s.

In general, the experimental HeCol cycle follows the appropriate ideal nonisothermal cycle. The lines that correspond to isosteric heating and cooling satisfactorily follow the shape of the theoretical weak and reach isosteres, which confirms the so-called "dead volume" effect to be negligible for the $LiCl/SiO_2$ adsorbent in a tested experimental rig [18]. However, the span between the experimental isosteres is visibly lower than for theoretical ones (Figure 7). This is because neither during the adsorption stage nor the desorption run does the adsorbent reach equilibrium, as the adsorption–desorption time is strongly restricted ($t_{ads/des}$ = 100–400 s). Indeed, the maximal change in uptake for the $LiCl/SiO_2$–CH_3OH working pair for the HeCol cycle reported in [19] is as high as Δw = 0.89 kg/kg. This is 1.8 times higher than the Δw experimentally obtained here for the consequent steady-state cycles with 400 s duration adsorption–desorption stages.

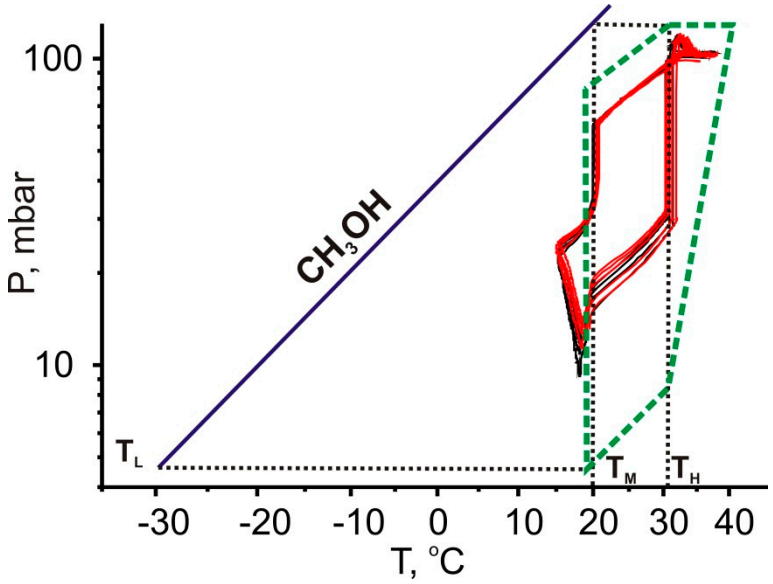

Figure 7. The ideal nonisothermal (dashed line) and experimental steady-state (solid lines) HeCol cycles with boundary temperatures of $T_L/T_M/T_H$ = –30/20/30 °C.

Figure 8a illustrates in detail the temporal evolution of temperature in adsorber A1 over the course of a single cycle. The inlet temperature (black line) is close to a meander-shaped line, with a 1200 s duration. This confirms that T1 and T2 thermostats equipped with 30 dm^3 buffer tanks are capable of satisfactorily compensating for the thermal effects of adsorption and desorption, keeping the inlet temperatures T_M and T_H within ± 1.5 °C of stability. The evolution of the outlet temperature (red line, Figure 8a) reflects the thermal effects that occur over the course of consecutive HeCol cycles. At first, this shows that both adsorption and desorption stages of the cycle are essentially nonisothermal. After the adsorption–desorption stage begins, the change in temperature between inlet and outlet reaches ΔT_{max} = 5 °C, and then it descends gradually until the moment when the gate valves are closed. On the other hand, the evolution of T_{out} shows that the durations of steps I, III, IV, and VI (Table 1) are enough for thermal equilibration of the adsorber after switching the HTF flow and after finishing the adsorption–desorption stage.

Over the course of a complete HeCol cycle, 4 thermal effects take place in a single adsorber (Figure 8b): (1) heat consumption Q(−) for isosteric heating of the adsorber from T_M up to T_H; (2) heat release Q_{ads} due to adsorption; (3) heat release Q(+) during isosteric cooling from T_H down to T_M; and (4) heat consumption Q_{des} for adsorbent regeneration. Both Q(−) and Q(+) are about 90–100 kJ, a value almost 3 times less than the heat of adsorption–desorption. Detailed analysis of inert thermal masses contributing to Q(−) and Q(+) is presented in [11], giving the sensible heat needed for isosteric heating of ≈ 80 kJ. The rest (≈ 10–20 kJ) is tentatively attributed to the pipelines, flanges, and fittings, which were not taken into consideration. The cumulative heat effects over the whole steady-state cycling at $t_{ads/des}$ = 400 s are summarized in Table 3.

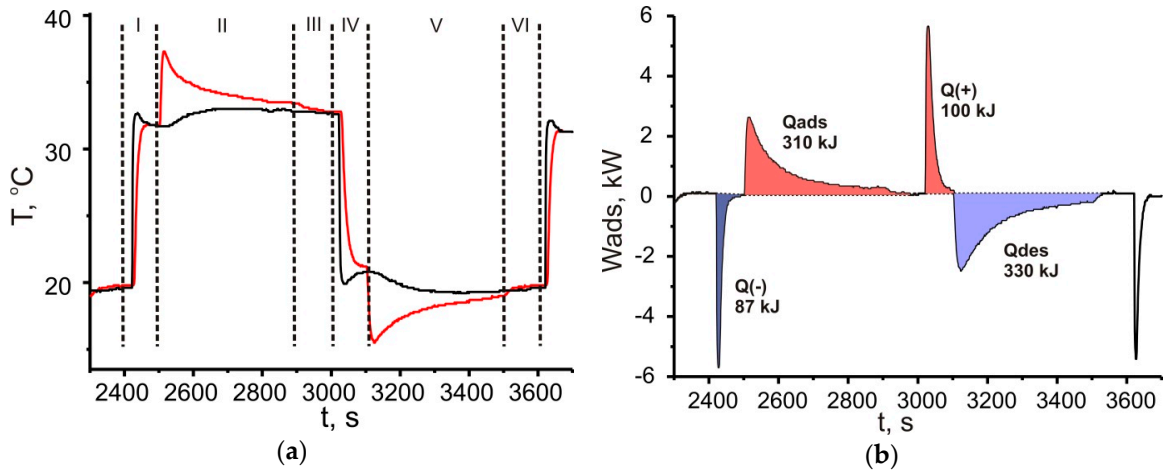

Figure 8. Evolution of inlet (black) and outlet (red) temperatures (**a**) and heat flow (**b**) for adsorber A1 over the course of a complete cycle, where $t_{ads/des}$ = 400 s. Stages I–VI are given in Table 1.

Table 3. The cumulative heat effects and heat balance for 4 consecutive steady-state cycles at $t_{ads/des}$ = 400 s.

Temperature Level	Heat Consumption		Heat Release	
	Source	Q, kJ	Source	Q, kJ
Useful heat (30 °C)	Isosteric heating	Q(−) = 700	Adsorption	Q_{ads} = 2480
Low potential heat source (20 °C)	Evaporation Regeneration	Q_{ev} = 2170 Q_{des} = 2650	Isosteric cooling	Q(+) = 800
Ambient air (−30 °C)	-	-	Condensation	Q_{con} = 2150
Total:		5520 kJ		5430 kJ
Heat balance:	ΔQ = **−90 kJ**		$\Delta Q/\Sigma Q$ = 90/5500 × 100% = **1.6%**	

3.2. Heat Balance and Performance Evaluation

Table 3 demonstrates that heat consumption and heat release in the tested AHT compensate each other with good accuracy. This shows that (a) both experimental and data evaluation procedures are correct and (b) heat losses in the experimental rig are negligible. The average amount of methanol exchanged per cycle over the whole steady-state period (4 consecutive and repeatable cycles) can be easily calculated by taking into account the isosteric heat of methanol adsorption on the $LiCl/SiO_2$ composite (ΔH_{ads} = 1.3 × 10^6 J/kg [15]):

$$\Delta w = Q_{ads}/(\Delta H_{ads} \times \mathrm{m} \times 4) = 0.48 \text{ kg/kg}. \quad (4)$$

This is in line with Δw = 0.49 kg/kg obtained previously for evaporation (Equation (3)). As the total duration of the steady-state cycles is t_{ss} = 4 × 1200 s = 4800 s, the specific adsorption power generated continuously in adsorbers A1 and A2 is as high as:

$$SP_{ads} = Q_{ads}/(t_{ss} \times m) = 520 \text{ W/kg}. \quad (5)$$

However, a part of the adsorption heat generated in the adsorbers is consumed for isosteric heating Q(−); thus, the specific useful power delivered to consumer SP_{us} becomes visibly less than SP_{ads}, namely:

$$SP_{us} = (\mathrm{Q_{ads}} - \mathrm{Q(-)})/(\mathrm{t_{ss}} \times \mathrm{m}) = 350 \text{ W/kg}. \quad (6)$$

It is worth noting that the useful heat generated continuously in the tested experimental rig is of a commercial value (T_H = 30 °C) and can be utilized, for example, for floor heating. On the other hand, both the low potential heat source (T_M) and heat sink (T_L) are considered as natural thermostats, which are available for free. Of course, besides these "free" heat sources and sinks, electric energy is necessary to pump the heat transfer fluid inside the heat exchangers, and to operate the valves and gates. The electric power of pumps M1–M4 is 15 W, as specified by the manufacturer; hence, the electricity consumption required to pump the thermal liquid is 60 W. The electromechanical gate valve consumes 10 W in an opened state; thus, according to Table 1, the average electric power required to activate the gates over the course of the tests is 20 W. The ball valves v1–v8 are equipped with 7 W electrical actuators; however, the valves are in use only twice each cycle during for ≈ 10 s, consuming on average (2.7 W × 8 × 10 s)/(1200 s) ≈ 1 W, which can be neglected. As a result, the electric efficiency of the tested experimental rig can be estimated as

$$\eta = (\text{useful thermal power})/(\text{electricity consumption}) = 350\ \text{W}/(60\ \text{W} + 20\ \text{W}) = 4.4 \quad (7)$$

The above is very encouraging and means HeCol is competitive with commercial climatic compression systems [20].

The second law efficiency for the studied HeCol cycle according to [11] is as high as

$$\eta_{SLT} = (1/T_L - 1/T_M)/(1/T_L - 1/T_H) = 0.86 \quad (8)$$

and represents the maximal theoretical efficiency of the adsorption heat amplifier with $T_L/T_M/T_H$ = −30/20/30 °C boundary temperatures. The data listed in Table 3 demonstrates that the experimental thermal performance η_{exp} of the tested AHT:

$$\eta_{exp} = (Q_{ads} - Q(-))/(Q_{des} + Q_{ev} - Q(+)) = 0.44 \quad (9)$$

is almost half that of η_{SLT} (Equation (8)). Obviously, the reason for the efficiency reduction is the fact that no internal recuperation of heat is realized in the tested experimental rig. As was mentioned above, a part of the adsorption heat produced at T_H is utilized for isosteric heating Q(−), whereas heat Q(+) released during isosteric cooling remains in a circuit connected with the source of low potential heat at T_M. Evidently, proper organization of internal heat recuperation could result in mutual compensation of Q(+) and Q(−), giving a formal thermal efficiency

$$\eta_{ads} = Q_{ads}/(Q_{des} + Q_{ev}) = 0.51 \quad (10)$$

that is close to the formal cycle efficiency previously reported for a single-bed HeCol prototype [11].

3.3. *Effect of Cycle Duration*

In the final part of this paper, the effect of adsorption–desorption duration (100–400 s) on the performance of the experimental HeCol rig is studied. All other parameters are fixed, as is reported in Table 1.

Figure 9 shows that the longer the adsorbent bed is in contact with the condenser and evaporator, the higher the amount of methanol exchanged Δw in the steady-state HeCol cycle. Indeed, with an increase of adsorption–desorption time $t_{ads/des}$ from 100 to 400 s, Δw rises gradually from 0.2 kg/kg up to 0.49 kg/kg.

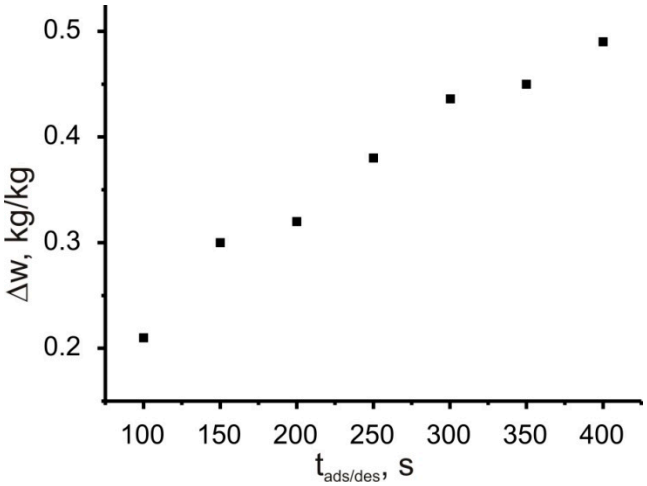

Figure 9. The amount of methanol exchanged in a cycle for different durations of the adsorption–desorption stage.

Hence, with longer $t_{ads/des}$, the heat released at adsorption stage Q_{ads} may increase as well. On the other hand, the higher the duration of adsorption–desorption, the longer the total cycle. As a result, the specific adsorption power SP_{ads} remains approximately constant (Figure 10) over a whole range of $t_{ads/des}$ within the specified experimental error range (Table 2). The specific useful power SP_{us} is visibly lower than SP_{ads}, especially at lower $t_{ads/des}$ (Figure 10). This is not surprising when considering that a part of the heat generated at the adsorption stage is utilized instantly for isosteric heating Q(−). The shorter the adsorption–desorption time, the lower the adsorption heat Q_{ads}, whereas Q(−) remains almost constant, which leads to a drop of useful heat

$$Q_{us} = Q_{ads} - Q(-) \tag{11}$$

and consequently of specific useful power SP_{us} (Equation (6)). At larger $t_{ads/des}$, both Δw (Figure 9) and Q_{ads} increase and a relative part of Q(−) is reduced in comparison with the heat of adsorption. On the other hand, the increase of Q_{ads} with further adsorption–desorption prolongation, is tentatively compensated by the increase in total cycle duration. As a result, the specific useful power SP_{us} approaches a constant at $t_{ads/des} > 250$ s (Figure 10).

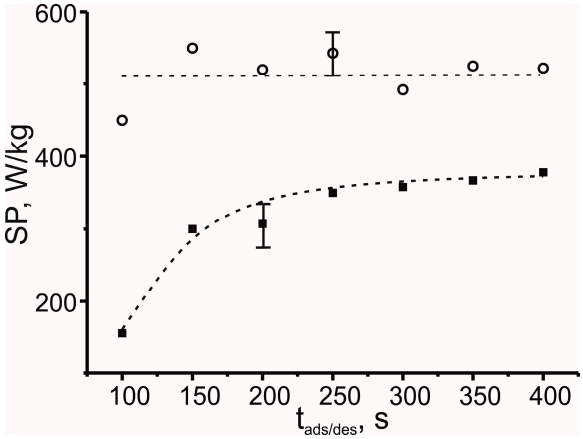

Figure 10. Specific adsorption power SP_{ads} (open symbols) and specific useful power SP_{us} (solid symbols) vs. adsorption–desorption time.

Evidently, the role of the complex interplay between Δw, Q_{ads}, Q(−), $t_{ads/des}$, and the total cycle time in the AHT performance should be the subject of further investigations and analysis. Besides this, the tendencies disclosed here for experimental and useful power turned out to be valid for the thermal efficiency (Figure 11) of the tested HeCol experimental rig. Namely, the formal efficiency η_{ads} remains almost constant within $t_{ads/des}$ = 100–400 s, whereas the experimental efficiency rises and approaches a constant η_{exp} = 0.45 ± 0.02 when the duration of the adsorption–desorption stage is longer than 200–250 s.

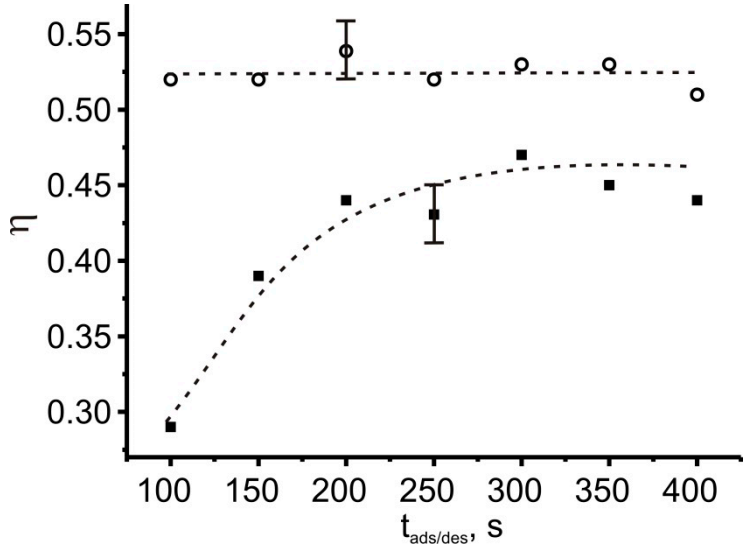

Figure 11. Variation of experimental (closed symbols) and formal (opened symbols) thermal efficiency with change in the duration of the adsorption–desorption stage.

Both the formal and experimental efficiencies achieved in the tests are roughly half of the upper limit η_{SLT} = 0.86 for heat machines operating over the boundary cycle temperatures of $T_L/T_M/T_H$ = –20/20/30 °C. Evidently, this is due to the fact that the tested AHT operates under nonisothermal and nonequilibrium conditions, resulting in entropy generation [11]. However, room for further improvement of the experimental rig and HeCol cycle still exists. The first and quite evident step is proper organization of the internal heat recuperation, which could potentially lead to increasing both the efficiency and specific power. The second possibility for growing the specific power is the optimization of the durations of stages I–VI. Figure 8b clearly shows that shortening the stages of thermal equilibration (III, VI) potentially could lead to a 10%–15% rise in *SP*. Nevertheless, the results obtained in the preliminary tests are very promising and demonstrate the potential for applying HeCol for energy saving.

4. Conclusions

In this study, a full scale lab prototype of an adsorptive heat transformer was designed, built, and tested under consecutive cycles of ambient heat upgrading. The test rig consisted of two adsorbers, a condenser, and an evaporator, and was loaded with 1 kg of the composite methanol sorbent $LiCl/SiO_2$. The adsorbers operated in an opposite mode that insured a continuous heat generation of 520 W under steady-state cycling for 1–1.5 h. The experimental and formal thermal performances were shown to be 0.44 and 0.51, respectively. Considering the heat sink and heat source as natural thermostats available for free, the electric performance of the tested prototype is as high as 4.4, showing good potential for practical realization of the HeCol concept. The suggestions for further improvements were outlined and discussed.

Author Contributions: All the work was done by the author, including the design and tests of the prototype, data treatment, and manuscript preparation.

Funding: This research was funded by the Russian Science Foundation, grant number 16-19-10259.

Acknowledgments: The author thanks A.A. Zlobin for synthesis of the adsorbent, A.I. Lysikov for his contribution in developing the control software and hardware, and L.G. Gordeeva and Y.I. Aristov for fruitful discussions.

Conflicts of Interest: The author declares no conflict of interest.

Abbreviations

Nomenclature:

ADC	analog-to-digital converter
AHT	adsorptive heat transformation/transformer
Cp	specific heat, J/gK
f	flow rate, L/h
H	enthalpy, J/kg
HEx	heat exchanger
HTF	heat transfer fluid
m	mass, kg
P	pressure, mbar
Q	heat, J
SP	specific power, W/kg
t	time, s
T	temperature, °C, K
w	uptake, kg/kg
W	power, heat flux, W

Greek symbols:

δ	relative error, %
ρ	density, g/cm^3
Δ	increment
ε	absolute error, K, g/cm^3
η	efficiency

Subscripts:

ads	adsorber, adsorption
cond	condenser, condensation
des	desorption
ev	evaporator, evaporation
H	high
in	inlet
L	low
max	maximal
M	middle
out	outlet
SLT	second law of thermodynamics
ss	steady-state
us	useful

References

1. Meunier, F. Adsorption heat powered heat pumps. *Appl. Therm. Eng.* **2013**, *61*, 830–836. [CrossRef]
2. Deng, J.; Wang, R.Z.; Han, G.J. A review of thermally activated cooling technologies for combined cooling, heating and power systems. *Prog. Energy Combust.* **2011**, *37*, 172–203. [CrossRef]
3. Wang, R.Z.; Xu, Z.Y.; Pan, Q.W.; Du, S.; Xia, Z.Z. Solar driven air conditioning and refrigeration systems corresponding to various heating source temperatures. *Appl. Energy* **2016**, *169*, 846–856. [CrossRef]

4. Sapienza, A.; Palomba, V.; Gulli, G.; Frazzica, A.; Vasta, S.; Freni, A. A new management strategy based on the reallocation of ads-/desorption times: Experimental operation of a full-scale 3 beds adsorption chiller. *Appl. Energy* **2017**, *205*, 1081–1090. [CrossRef]
5. Xu, S.Z.; Wang, L.W.; Wang, R.Z. Thermodynamic analysis of single-stage and multi-stage adsorption refrigeration cycles with activated carbon–ammonia working pair. *Energy Convers. Manag.* **2016**, *117*, 31–42. [CrossRef]
6. Sah, R.P.; Choudhury, B.; Das, R.K. A review on low grade heat powered adsorption cooling systems for ice production. Renew. *Sustain. Energy Rev.* **2016**, *62*, 109–120. [CrossRef]
7. Wang, R.Z.; Ge, T.S.; Chen, C.J.; Ma, Q.; Xiong, Z.Q. Solar sorption cooling systems for residential applications: Options and guidelines. *Int. J. Refrig.* **2009**, *32*, 638–660. [CrossRef]
8. Cabeza, L.F.; Solé, A.; Barreneche, C. Review on sorption materials and technologies for heat pumps and thermal energy storage. *Renew. Energy* **2017**, *110*, 3–39. [CrossRef]
9. Kohlenbach, P.; Jakob, U. *Solar Cooling: The Earthscan Expert Guide to Solar Cooling Systems*, 1st ed.; Routledge: New York, NY, USA, 2014; pp. 147–160.
10. Aristov, Y.I. "Heat from cold"—A new cycle for upgrading the ambient heat: Adsorbent optimal from the dynamic point of view. *Appl. Therm. Eng.* **2017**, *124*, 1189–1193. [CrossRef]
11. Aristov, Y.I. A new adsorptive cycle "HeCol" for upgrading the ambient heat: The current state of the art. *Int. J. Refrig.* **2019**, *105*, 19–32. [CrossRef]
12. Gordeeva, L.G.; Tokarev, M.M.; Aristov, Y.I. New adsorption cycle for upgrading the ambient heat. *Russ. Theor. Found. Chem. Technol.* **2018**, *52*, 195–205. [CrossRef]
13. Tokarev, M.M.; Grekova, A.D.; Gordeeva, L.G.; Aristov, Y.I. A new cycle "Heat from Cold" for upgrading the ambient heat: The testing a lab-scale prototype with the composite sorbent CaClBr/silica. *Appl. Energy* **2018**, *211*, 136–145. [CrossRef]
14. Gordeeva, L.G.; Tokarev, M.M.; Shkatulov, A.I.; Aristov, Y.I. Testing the lab-s-cale "Heat from Cold"prototype with the "LiCl/silica -methanol"working pair. *Energy Convers. Manag.* **2018**, *159*, 213–220.
15. Gordeeva, L.G.; Freni, A.; Krieger, T.A.; Restuccia, G.; Aristov, Y.I. Composite sorbents "LiCl in silica gel pores": Methanol sorption equilibrium. *Microporous Mesoporous Mater.* **2008**, *112*, 254–261. [CrossRef]
16. SecCool. Available online: https://www.ipu.dk/products/seccool/ (accessed on 23 September 2019).
17. Weast, R.C. *Handbook of Chemistry and Physics*, 84th ed.; Lide, D.R., Ed.; CRC: Boca Raton, FL, USA, 2004.
18. Tokarev, M.M.; Veselovskaya, J.V.; Yanagi, H.; Aristov, Y.I. Novel ammonia sorbents "porous matrix modified by active salt" for adsorptive heat transformation: 2.Calcium chloride in ACF felt. *Appl. Therm. Eng.* **2010**, *30*, 845–849. [CrossRef]
19. Tokarev, M.M.; Zlobin, A.A.; Aristov, Y.I. A new version of the large pressure jump (T-LPJ) method for dynamic study of pressure-initiated adsorptive cycles for heat storage and transformation. *Energy* **2019**, *179*, 542–548. [CrossRef]
20. Martinopoulos, G.; Papakostas, K.T.; Papadopoulos, A.M. A comparative review of heating systems in EU countries, based on efficiency and fuel cost. *Renew. Sustain. Energy Rev.* **2018**, *90*, 687–699. [CrossRef]

© 2019 by the author. Licensee MDPI, Basel, Switzerland. This article is an open access article distributed under the terms and conditions of the Creative Commons Attribution (CC BY) license (http://creativecommons.org/licenses/by/4.0/).